How the range of pair interactions governs features of multidimensional potentials

Paul A. Braier, R. Stephen Berry, and David J. Wales

Citation: The Journal of Chemical Physics **93**, 8745 (1990); doi: 10.1063/1.459263
View online: http://dx.doi.org/10.1063/1.459263
View Table of Contents: http://scitation.aip.org/content/aip/journal/jcp/93/12?ver=pdfcov
Published by the AIP Publishing

How the range of pair interactions governs features of multidimensional potentials

Paul A. Braier and R. Stephen Berry
Department of Chemistry, The University of Chicago, 5735 South Ellis Avenue, Chicago, Illinois 60637
David J. Wales
University Chemistry Laboratories, Lensfield Road, Cambridge CB2 1EW, United Kingdom

(Received 12 March 1990; accepted 4 September 1990)

By using the pairwise Morse potential as the principle vehicle we have explored the influence of the range of the pair potential on the structure of multidimensional potential-energy surfaces. A scaling relation and a set of reduced units are presented for the homoatomic pairwise-additive Morse potential. The reduced potential has one free parameter, βr_0 or ρ_0, regulating the range of interaction. Based on several diatomic species, the chemically important range of ρ_0 is approximately $2 \leqslant \rho_0 \leqslant 7$. The number of geometrically distinct minima and transition states depends on ρ_0; the larger is ρ_0, the narrower is the potential and the greater is the number of geometrically different minima. To illustrate this we found all minima and important low-energy transition states for the Morse six-and seven-particle clusters as functions of ρ_0 in its chemically interesting range. From these the dominant mechanisms of isomerization of six- and seven-particle clusters are inferred and compared with experimental and theoretical results for main-group and transition-metal clusters. A nomenclature for saddle points and isomerizations is introduced. The saddle regions of the potentials reveal the dominance of diamond–square–diamond and edge-bridging mechanisms. Knowledge of the stationary points and rearrangement mechanisms allows us to determine the proper molecular symmetry groups and the topologies of the potential-energy surfaces at any arbitrary energy.

I. INTRODUCTION

The structures available to any cluster or molecule are determined by the nature of the interatomic potential. The dynamics that a cluster or molecule undergoes, all of the bends, stretches, torsions, and other vibrations available to it are merely walks upon this potential surface. The most important features of the surface are its stationary points: the minima and the saddles at which the net force vanishes for every atom of the molecule. Each molecule, with its own particular potential energy surface, has its own particular set of stationary points.

The potential-energy surface of a many-atom system is a very complicated function of the interatomic distances. In some systems, such as clusters of rare-gas atoms, the internuclear pairwise additive terms dominate and largely determine the features of the potential surface; many other systems have appreciable nonpairwise additive contributions to the potential due to delocalized electrons, to directional bonding, to Jahn–Teller distortions, and to other effects. Nevertheless, the assumption of an atomic pairwise-additive potential surface is a useful first approximation in the study of a great many molecules and clusters.

This study is intended to probe general characteristics of potential surfaces on what we may call a *regional* scale. We are interested in more than the local portions of surfaces which are explored by molecules in their lowest vibrational states, but not yet in the global topology of the entire surface and of the full mapping of the connectivity of all the potential wells. (This work does lead directly into the study of the global structure of many-dimensional potentials; a following publication will describe how to extend this work to find the global structure.) More specifically, we are interested in finding the kinds of potential minima on a multidimensional surface and the saddles, or at least the important saddles, that connect those minima. Most of the analysis is based on pairwise-additive Morse interactions partly because of the utility[1] of such potentials and partly because of their convenience for the kind of generic study we present here, namely for studying the variation of features of the potential surface with variations in the range of the pairwise interaction. Hence our viewpoint is intended to be general, but our means of establishing the points of interest are through specific illustrations.

The Morse[2] and the Lennard-Jones[3] potentials are two of the most frequently used for pairwise interatomic interactions. These two pair potentials share a common form, namely $V(r) = \epsilon([g(r) - 1]^2 - 1)$ where ϵ is the classical dissociation energy, or well depth, and $g(r)$ is a function that grows large as r goes to zero, and that monotonically and asymptotically decreases to zero as r goes to infinity. For the Lennard-Jones potential $g(r) = (r_0/r)^6$ and for the Morse potential $g(r) = e^{-\beta(r - r_0)}$ where β regulates the well width in the latter and r_0 is the equilibrium diatomic separation for both.

The Lennard-Jones potential is often used to model systems held together by van der Waals forces because of the r^{-6} decay, while the Morse potential, with its exponential decay, is more appropriate for covalently bonded systems.

Since the Lennard-Jones potential has only two parameters it can be expressed in a set of reduced units so that all systems obeying this potential exhibit identical behavior when expressed in terms of those units. The Morse potential has the additional parameter β that allows for an indepen-

dent choice of well width. For this reason, the Morse potential, unlike the Lennard-Jones potential, does not have such a simple reduced form or scaling law. We shall see, however, that it does obey a slightly more complex scaling law which can be exploited to characterize the potential surface.

The many-particle pairwise-additive Morse potential is a model for superposed isotropic atom–atom potentials. We shall show below that in its reduced form the potential has only one parameter, designated ρ_0, which determines the range of the interactions. Systems with large values of ρ_0 are tightly bound rigid systems with high vibrational frequencies. Systems with small values of ρ_0 are less tightly bound and have lower frequencies of vibration.

We expect that the stationary points of the molecular potential-energy surface must be strongly influenced by the nature of the interatomic interactions. The stationary points, in turn, determine the structures and dynamics available to the system. In the present work we examine this relationship by studying how the stationary points of two Morse systems are affected by systematic changes in the range of the interactions.

The systems we shall study are the two clusters M_6 and M_7, where "M" refers to "Morse," not "metal." These clusters are small enough that we can classify their important stationary points easily, yet large enough for their potential surfaces to be interesting.

The important rearrangement mechanisms are discussed in Sec. II. In Sec. III we express the Morse potential in a set of reduced units which allow it to be written as a one-parameter potential. The methods used to explore the potential surfaces are discussed in Sec. IV, followed by presentation of results in Sec. V. In Sec. VI we discuss these results and compare the Morse potential to the Lennard-Jones. We also show how knowledge of the topology of the potential surface can be utilized to determine the effective molecular symmetry group of a cluster or molecule. Our conclusions are presented in Sec. VII and formulas for the first and second derivatives of the Morse potential are given in the Appendix.

II. REARRANGEMENT MECHANISMS

Clusters of the transition metals, main-group elements, and rare gases all tend to adopt deltahedral geometries, wherein all the faces are triangular. Due to the large number of nearest-neighbor contacts characteristic of deltahedra, these configurations should be favored in the absence of strong repulsive many-body contributions to the potential. Rearrangements among the deltahedral minima have been observed to proceed mainly by two distinct mechanisms.

Lipscomb's diamond–square–diamond (DSD) process,[4] shown in Fig. 1(a), has been used as the fundamental rearrangement mechanism[5] to rationalize the rearrangement rates of borohydrides. An ideal single-step DSD process involves four neighboring atoms arranged in a rhombus (the diamond) in which there is a bond between the two atoms on the short diagonal, the critical edge. As the cluster proceeds away from the local minimum the long diagonal shortens and the short diagonal lengthens until the four atoms form a square at the transition state. As the cluster

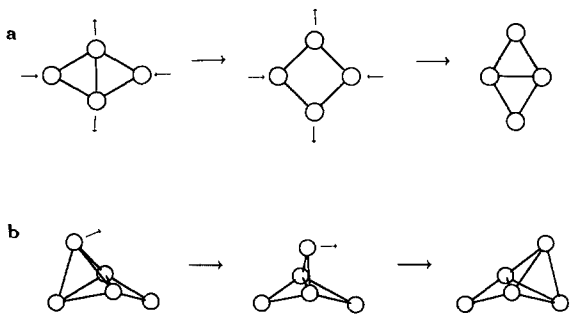

FIG. 1. Two reaction mechanisms. (a) The diamond-square–diamond (DSD) process; (b) the edge-bridging process.

progresses toward the product structure, the two diagonals continue to change lengths until what was the short diagonal becomes the long diagonal and vice versa. Of course, the four atoms that form the critical face for this process are not the only atoms involved. As the transition progresses all the other atoms in the cluster relax in such a way as to minimize the energy. If a DSD process takes a cluster from one structure to a geometrically equivalent one, then the critical edge is termed "degenerate."[6]

In practice, the critical face of a DSD process need not be a rhombus; it need not even be planar. Similarly, the critical face midway through the process need not be a square. Furthermore, the term "bond" is used in its generalized sense to include nearest-neighbor contacts or edges; it does not imply the existence of a two-center, two-electron bond.

Another possible basic rearrangement mechanism is Johnson's edge-bridging process,[7] which is shown in Fig. 1(b). This mechanism involves a surface atom detaching itself from the cluster and moving from one face of the cluster to an adjacent face. The transition state for this process has the mobile atom straddling the edge between the initial and destination faces, hence the name "edge bridge." This mechanism is generally higher in energy than the single DSD mechanism, as recent studies have shown.[8,9] Furthermore, some of the edge-bridging transition states found using the Lennard-Jones potential for argon cease to be stationary points of any order when a more accurate potential is used.[10]

These rearrangement mechanisms have two especially intuitively appealing characteristics: first, they both involve breakage of a minimum number of nearest-neighbor distances, and second, they both only entail a minimal movement of the constituent atoms. As we show below, even when more complicated rearrangements occur, they can be cast in terms of the above processes, especially the DSD process.

III. THE MORSE POTENTIAL

Write the N-particle pairwise additive Morse potential as

$$V_M = \epsilon \sum_{i<j} (e^{-2\beta(r_{ij}-r_0)} - 2e^{-\beta(r_{ij}-r_0)}), \tag{1}$$

where $r_{ij} = |\mathbf{r}_i - \mathbf{r}_j|$ is the distance between atoms i and j. The $3N$ elements of the gradient are then given by

$$\frac{\partial V_M}{\partial x_n} = -2\beta\epsilon \sum_{i\neq n} \frac{x_{ni}}{r_{ni}} e^{-\beta(r_{ni}-r_0)}(e^{-\beta(r_{ni}-r_0)} - 1) \tag{2}$$

with similar definitions for the y and z directions. We define $x_{ni} = x_n - x_i$, $y_{ni} = y_n - y_i$, and $z_{ni} = z_n - z_i$ to be signed distances.

Let us select an arbitrary real positive number k. Now expand (or contract) our N-atom system and potential by multiplying *every* distance, including r_0, by k. Next, change the Morse well width by replacing every occurrence of β with β/k. Obviously, after this is done, the product $r_0\beta$ will not have changed. Since $r_0\beta$ is a dimensionless product in the exponential, the energy of the system will not have changed either, but the value of each element of the gradient will have changed by a constant factor of $1/k$. If a similar procedure is followed for the elements of the Hessian matrix (see the Appendix for the Morse second derivatives), we see that the elements are scaled by a constant factor of $1/k^2$. The importance of the first result is that any two N-particle systems with identical $r_0\beta$ must have geometrically equivalent stationary points since the gradient, by definition, vanishes at these points. The second result strengthens the first, for not only must the stationary points remain, but the rank of each point must remain unchanged, so that the stationary points of the Morse potential can be studied by varying only one parameter, namely $r_0\beta$. Henceforth we define $\rho_0 = r_0\beta$.

We now transform the Morse potential to reduced units. The unit of energy is ϵ, the diatomic well depth, and the reduced potential is then written $\hat{V}(\rho_0;\rho)$. The unit of length will be $1/\beta$, and we shall denote the reduced lengths by $\rho = \beta r$. The appropriate unit of time becomes $\tau = (m/4\epsilon\beta^2)^{1/2}$ where m is the mass of a constituent atom.

We have calculated the value of ρ_0 for several homoatomic systems based upon data compiled[11] for their respective diatomics. The expression for ρ_0 is[12]

$$\rho_0 = r_0\omega_e\left(\frac{c\pi\mu}{\hbar D_e}\right)^{1/2}, \tag{3}$$

where ω_e is the vibrational constant, c is the speed of light, μ is the reduced mass, and D_e is the classical dissociation energy. One should not consider these values, which are listed in Table I, to be necessarily the "correct" parameters for a particular many-atom Morse cluster; there is evidence that for clusters, the average equilibrium nearest-neighbor distance increases with increasing nuclearity,[13] mainly due to surface effects.[14] How the force constants change with changing nuclearity is less clear. Nonetheless, the values of ρ_0 in Table I should be considered as good first approximations.

TABLE I. Morse parameters for several diatomic molecules. Values for the well depth, r_0 and β, are from Huber and Herzberg (Ref. 11).

Diatomic species	Well depth (eV)	r_0 (Å)	β (Å^{-1})	ρ_0
Ne_2	0.002 02	1.75	1.17	2.05
Ar_2	0.010 51	3.76	1.52	5.72
Kr_2	0.015 7	4.03	1.69	6.81
Xe_2	0.023 0	4.36	1.53	6.67
Cu_2	2.03	2.22	1.41	3.13
Ag_2	1.66	2.47	1.49	3.68
Au_2	2.30	2.47	1.69	4.18
Mg_2	0.050 1	3.89	1.07	4.16
Ca_2	0.129	4.28	1.10	4.70

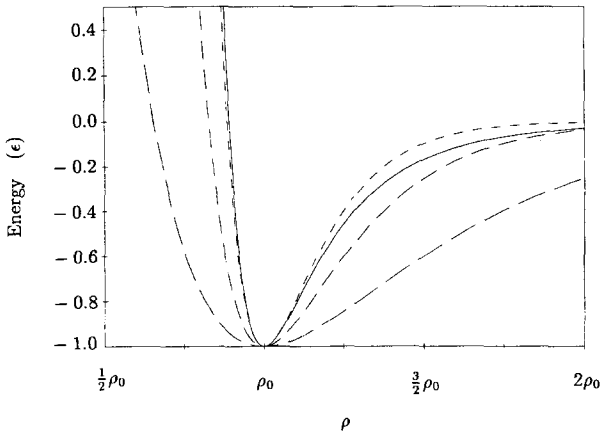

FIG. 2. Plots of the Morse potential vs r in units of ρ_0. Short-dashed line, $\rho_0 = 6$; medium-dashed line, $\rho_0 = 4$; long-dashed line, $\rho_0 = 2$. A Lennard-Jones potential (solid line) is also plotted for comparison with the Morse curves. The curvature at the bottom of the well for $\rho_0 = 6$ matches that of the Lennard-Jones potential.

In Fig. 2 we have plotted the reduced Morse potential for three values of ρ_0. The width of the well measured at any negative energy is proportional to ρ_0. When $\rho_0 = 6.0$ the curvature at the bottom of the diatomic well equals that of the Lennard-Jones potential, so for this value the reduced unit of time of both potentials are identical.

The range of physically relevant ρ_0 appears to be approximately the interval $1.5 < \rho_0 < 7$. At values of ρ_0 less than about 1.5 the Morse potential itself becomes physically unrealistic since $\hat{V}(\rho_0 = 1.5; \rho = 0) \approx 10$, i.e., the potential at zero separation is only about 10 times as high as the diatomic well is deep. While this is high enough to simulate actual interatomic repulsive potentials, for smaller ρ_0 other complications set in because of this,[15] so $\rho_0 \approx 1.5$ should be considered as a lower physically realistic limit. As ρ_0 increases, $\hat{V}(\rho_0; \rho = 0)$ increases exponentially, so this ceases to be of any real concern. A large value of ρ_0, on the other hand, results in a very tightly bound system with very high vibrational frequencies, becoming much higher than any molecule can actually exhibit. This upper limit is less well defined than the lower limit, but based on Table I, $\rho_0 \approx 7$ appears to be a plausible value. For completeness, we have examined the potential for $0 < \rho_0 < 10$.

For a very-long-ranged potential, corresponding to small ρ_0, the concepts of interatomic bonds, bond breakage, and bond formation become rather ambiguous. Suppose we have a diatomic molecule whose atoms are at equilibrium separation. Whereas an increase in separation of, say, 10%, from equilibrium results in over a 20% increase in potential energy when $\rho_0 = 6$, the same increase in bond length results in just over a 3% increase in potential for $\rho_0 = 2$. The behavior for large ρ_0 agrees nicely with our traditional concept of an interatomic bond, but one would be hard pressed to say that the case of small ρ_0 simulates a chemical bond; the longer-range potential is just too insensitive to changes in inter-

nuclear separation and too sensitive to second-nearest neighbors. Since bonds between nearest neighbors become increasingly ill-defined as ρ_0 decreases, the DSD and edge-bridging rearrangement mechanisms previously discussed may lose their special roles for systems with small ρ_0, or for systems with long-range potentials generally. This follows because both the DSD and the edge-bridging processes involve minimal bond-breaking perturbations; orbital symmetry aside, this criterion appears to be of utmost importance in boranes.[5] However, as the potential becomes increasingly long ranged, simultaneous breakage of multiple nearest-neighbor contacts becomes energetically less unfavorable.

IV. METHOD

The reaction path must follow an evolving eigenvector of the Hessian,[16] the matrix of second derivatives of the potential energy. Hence a simple potential-energy maximization with an algorithm that follows such an eigenvector will allow us to locate the transition state if one exists for the particular normal mode chosen. Because any realistic potential has significant deviations from harmonicity, the "normal modes," the directions that diagonalize the Hessian, are not constant, but evolve continuously along the reaction path. In 1981, Cerjan and Miller[17] presented an algorithm that could follow such normal modes. Their method involves a quadratic approximation to the local potential-energy surface using the first and second derivatives of the potential energy. With a well-defined algorithm one can maximize the energy with respect to displacements along one particular normal mode while simultaneously minimizing the energy with respect to the other modes. Hence, starting from a local minimum the algorithm takes successive steps along the chosen normal coordinate until either a saddle is reached or it is determined that no saddle exists for that mode.

Some recent studies[8-10,18] have shown that the approach is remarkably successful when applied to a very wide variety of different potential-energy surfaces. For the present work the optimizer from the ACES quantum chemistry package[19] was modified to treat the Morse clusters described above using analytic gradients and Hessians. More details have been given elsewhere[8,9] and the approaches used in the present study were very similar.

In some cases we found it helpful to apply symmetry constraints to the clusters in order to facilitate saddle searches and to search for higher-order saddles. In these situations the optimized structures were then released from the constraints and independently tested to confirm both that the Hessian had the proper number of negative eigenvalues, and that the elements of the gradient were effectively zero. We determined reaction mechanisms by normal-mode analyses of the saddle points.

At intervals of $\rho_0/2$ we retested each minimum and saddle that we found until one of two situations arose: (1) we reached either $\rho_0 = 10$ or 0, in which case the search ended, or (2) we passed a critical value of ρ_0 beyond which the structure no longer corresponded to a low-order stationary point. In the latter case we determined this critical value of ρ_0 to ± 0.01 accuracy.

V. RESULTS

In this section we examine our illustrative examples of M_6 and M_7 first for their stationary points—minima and low-energy saddles—and then for the mechanisms that connect these minima. In order to make such examinations amenable to extensions to other systems, we introduce a nomenclature, in the context of the rearrangements of M_7, for classifying the saddles of a multidimensional potential. The sections dealing with rearrangements will be of interest to readers concerned with reaction mechanisms.

A. M_6 clusters: Stationary points

Only two minima were found for M_6 clusters in the physically significant range of ρ_0. These minima are shown in Fig. 3. For $\rho_0 > 4.10$ both minima appear and are the same as those found for the six-particle Lennard-Jones cluster.[20] The octahedron, point group O_h, is the global minimum throughout the range of ρ_0 considered. The other minimum, which we call the incomplete pentagonal bipyramid, can be thought of as a pentagonal bipyramid with one of the equatorial atoms missing. It can also be thought of as a bicapped tetrahedron or distorted octahedron, but as fivefold symmetry has been widely observed both experimentally[21] and theoretically[20,22] in small clusters, we prefer the first designation. These minima will be abbreviated as OCT(0) and IPB(0) respectively, where the zeros refer to the rank of the stationary point. See Table II for collected values of the minima of M_6 and M_7.

Figure 4 is a graph of the energy of the two minima plotted against ρ_0. Note that the curve for the octahedron asymptotically approaches integer values of the energy (measured in ϵ) as ρ_0 gets either very large or small. As ρ_0 grows large, the potential becomes increasingly short ranged so that only nearest neighbors contribute to the energy, and these contribute very nearly $-\epsilon$ each. The octahedron has 12 nearest-neighbor distances, so as ρ_0 gets large the energy tends to -12ϵ. As ρ_0 becomes small, however, the potential becomes very long ranged, so that every pair of atoms contributes $-\epsilon$ to the energy. Thus for small ρ_0 the energy approaches $-\epsilon N(N-1)/2$, or -15ϵ for M_6. The curve's asymptotes are therefore governed by two very different principles: the large ρ_0 asymptote is determined from the geometry of the particular structure while the small ρ_0 asymptote is solely determined by the number of atoms in the cluster.

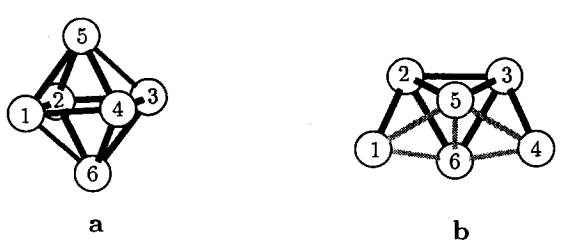

a b

FIG. 3. The M_6 minima. (a) Octahedron, OCT(0); (b) incomplete pentagonal bipyramid, IPB(0). The edges are highlighted for visualization purposes only. All configurations are for $\rho_0 = 10$.

TABLE II. The M_6 and M_7 minima. The minima are listed in order of increasing energy. The second column lists the minimum value of ρ_0 for which the structure exists. The fourth column gives the number of equivalent permutational isomers. The fifth column lists the minima that are directly connected to the minimum in question by a first-order saddle. The saddles for degenerate rearrangements when the global minimum is the sole minimum are not given. Otherwise, the connectivities are listed by increasing energy of the transition state.

Structure	$\rho_{0,\min}$	Point group	Number	Connectivity
M_6				
OCT(0)	···	O_h	30	12 IPB(0)
				8 OCT(0)
IPB(0)	4.10	C_{2v}	360	1 OCT(0)
				2 IPB(0)
M_7				
PBP(0)	···	D_{5h}	504	10 COCT(0)
				10 SKEW(0)
				10 IST(0)
				20 SKEW(0)
COCT(0)	1.86	C_{3v}	1680	3 PBP(0)
				3 IST(0)
				6 SKEW(0)
				3 COCT(0)
IST(0)	3.23	C_{3v}	1680	3 COCT(0)
				3 PBP(0)
SKEW(0)	3.74	C_s	5040[a]	2 COCT(0)
				2 PBP(0)
				2 SKEW(0)[b]
				1 SKEW(0)[b]
				2 PBP(0)
				2 SKEW(0)[b]

[a] There are actually 2520 permutational isomers of each enantiomer.
[b] This saddle is between different enantiomers.

The curve for the IPB(0) also approaches its expected energy as ρ_0 gets large, but comes to a sudden end at $\rho_0 = 4.10$. As ρ_0 decreases to this value the potential becomes sufficiently long ranged that the two far equatorial atoms are pulled toward each other and the structure collapses into an octahedron. It is interesting that the octahedron is still the global minimum whatever the range of the Morse potential. Not only is it a balanced structure[10,23] (so long as it corresponds to an electronically nondegenerate state), but it is deltahedral so that it has the maximum number of superficial nearest-neighbor contacts.

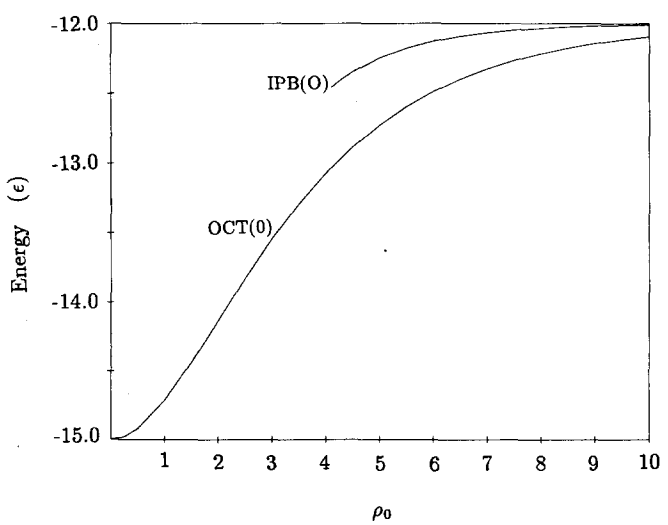

FIG. 4. Energies of the M_6 minima as functions of ρ_0.

Hoare[20] had reoptimized the Lennard-Jones minima using the Morse potential to determine which structures would survive; he found only one structure for M_6, the octahedron. This is to be expected since he used only the single value of $\rho_0 = 3.0$ for the Morse interaction.

To further expose the trends of the stationary points we found it convenient to define a new energy reference and a corresponding rescaling. In Fig. 5 we show the energies of the higher important stationary points relative to the global minimum energy now defined to be -1.00 for all values of ρ_0 and the dissociation limit of zero. Plotting the energies in this way makes it easy to see trends in barrier heights and relative stabilities of various structures.

The structures of the first-order saddles and a third-order saddle are shown in Fig. 6. Figure 6(a) is a picture of the IPB(1) saddle, which connects the OCT(0) and the IPB(0) and can be thought of as a slightly distorted IPB(0). The IPB(0) and IPB(1) structures are obviously not balanced structures since not all the atoms lie on rotation axes,[10,23] hence there is no reason to expect that they should be stationary points for all values of ρ_0. As ρ_0 decreases to the critical value of $\rho_0 = 4.10$ the IPB(0) and IPB(1) structures merge. At this point (see Fig. 7) the gradient still vanishes, but so does the eigenvalue associated with the eigenvector of

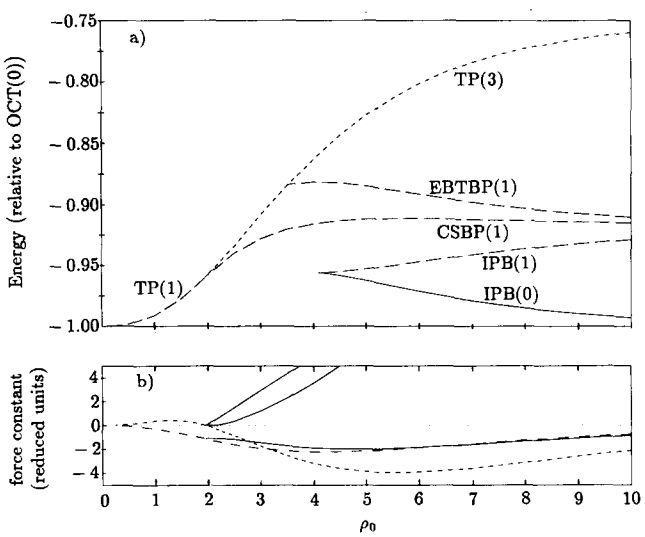

FIG. 5. (a) Energies of the stationary points of M_6 as functions of ρ_0. The energies are relative to the octahedron, the global minimum. Solid curves are minima, long-dashed curves are first-order saddles, and the short-dashed curve is the third-order saddle, TP(3). The curve corresponding to EBTBP(1) projects a distance of $0.01\rho_0$ beyond that of TP(3); those two curves do not merge. (b) Some force constants of the trigonal prism (dashed lines) and the capped square-based pyramid (solid lines) as functions of ρ_0. The two force constants of the TP transform as E'' (short-dashed line) and A_2' (long-dashed line). For $\rho_0 > 1.95$ the negative force constant of the CSBP(1) transforms as A'' and the two positive forces are of symmetry species A' (steeper line) and A''. The horizontal dotted line at zero is for reference.

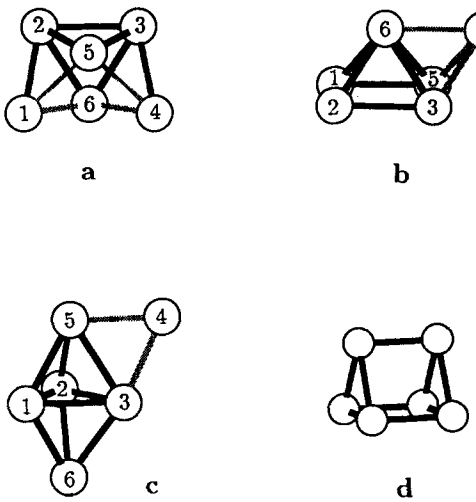

FIG. 6. The M_6 saddles ($\rho_0 = 10.0$). (a) Incomplete pentagonal bipyramid, IPB(1), which is a slightly distorted IPB(0); (b) capped square-based pyramid, the highlighted bonds emanate from the cap atom; (c) edge-bridged trigonal bipyramid, the highlighted bonds emanate from the edge-bridge atom; (d) trigonal prism, the edges are highlighted for visualization purposes only.

that mode. When this happens, the potential along that direction is dominated by a cubic term and the normal mode is no longer well defined. Such a bifurcation point, although interesting in its own right, actually has little significance in physical problems since the likelihood is zero that both linear and quadratic terms of the potential will vanish at any point for any molecule.[24]

B. M_6 clusters: Rearrangement mechanisms

The reaction mechanism for the OCT(0)–IPB(0) rearrangement is a DSD process. All 12 edges of the OCT(0) are equivalent, so each OCT(0) is connected by this process to 12 equivalent IPB(0) minima. In Fig. 3(a), a DSD process breaking the 1–4 edge leads to the structure in Fig. 3(b). For large ρ_0 the next highest-energy saddle is a capped square-based pyramid [Fig. 6(b)], designated CSBP(1). See Table III.

There are four equivalent degenerate edges in the IPB(0) shown in Fig. 3(b). The CSBP(1) serves as the transition state for the single DSD rearrangement. A DSD process on the 2–5 edge of the IPB(0) shown in Fig. 3(b) results

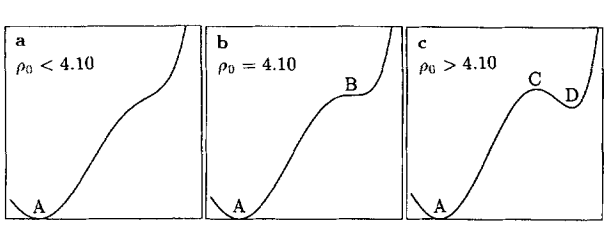

FIG. 7. A schematic drawing of the Morse potential along the OCT(0)–IPB(0) reaction coordinate for various values of ρ_0. (a) $\rho_0 < 4.10$; (b) $\rho_0 = 4.10$; (c) $\rho_0 > 4.10$. Structure A, octahedron OCT(0); structure B, a "merged" IPB(0) and IPB(1); structure C IPB(1); and structure D, IPB(0).

TABLE III. The M_6 saddles.

Structure	Point group	Number	Pathway	Range of ρ_0
IPB(1)	C_{2v}	360	OCT(0)–OCT(0)	$\rho_0 > 4.10$
CSBP(1)	C_s	720	IPB(0)–IPB(0)	$\rho_0 > 4.10$
			OCT(0)–OCT(0)	$1.95 < \rho_0 < 4.09$
EBTBP(1)	C_s	720	OCT(0)–OCT(0)	$\rho_0 > 3.54$
TP(1)	D_{3h}	120	OCT(0)–OCT(0)	$\rho_0 < 1.94$

in a transition state with the atoms labeled as in Fig. 6(b). A DSD process on the 3–5 edge leads to the same rearranged IPB(0) as the DSD on the 2–5 edge, but by a differently numbered saddle. For $\rho_0 < 1.95$ the trigonal prism TP(1) is a true saddle, distorting by the A_2' twisting mode into one of two octahedra. At $\rho_0 = 1.95$, the TP(1) becomes a third-order saddle because the force constants of the E'' mode that shears the prism (keeping triangular faces approximately parallel) go to zero there and are negative for larger ρ_0. Approximately, that same E''-mode distortion from the TP at $\rho_0 = 1.95$ takes the cluster to a true first-order saddle, a capped square-based pyramid CSBP(1). The CSBP(1) has no degenerate modes and only one negative force constant, which is related to the twisting mode of the triangular prism. The descendents in the CSBP(1) of the shear mode of the TP have positive force constants, which grow from zero at $\rho_0 = 1.95$. These force constants are illustrated in the small panel of Fig. 5(b). Incidentally, the negative force constants go to zero for both very small and very large ρ_0, because for small values the potential becomes flat everywhere, and for large values, except for close neighbors, the potential is flat for all atom pairs, including those whose relative motion determines the rearrangement path.

The rearrangement process for the OCT(0) via the TP(1) saddle is a face rotation in which opposite faces of the OCT(0) undergo a relative rotation of 120°. As implied by Lipscomb,[4] the face rotation may also be viewed as a concerted triple DSD process on, for example, the 1–6, 5–4, and 2–3 bonds. When $1.95 < \rho_0 < 4.10$ the OCT(0)–OCT(0) rearrangement occurs through the same mechanism, and the CSBP(1) saddle in this case can be thought of as a distorted TP(1) It is noteworthy that the octahedral borane $B_6H_6^{2-}$ is found to be stereochemically rigid, while there is evidence that platinum clusters composed of stacked triangular units such as $Pt_6(CO)_{12}^{2-}$ rearrange via low-energy trigonal twists.[25] This may be rationalized using orbital symmetry and electron-counting arguments,[25] but the "softer" potential-energy surface expected for metal–metal bonding would imply a smaller value of ρ_0 and also fits qualitatively with the results of the present model.

The highest-energy first-order saddle found in this study connects two OCT(0) structures to each other via an edge-bridging process. The transition state, shown in Fig. 6(c), is an edge-bridged triagonal bipyramid, EBTBP(1). To reach this structure from the OCT(0) of Fig. 3(a), the 1–4 and 6–4 edges must break and 2–4 and 6–4 edges are formed. On searching for an edge-bridging transition state with a bridged equatorial bond the structure immediately

collapses into an octahedron, so this alternate mechanism does not appear to exist.

C. M_7 clusters: Stationary points

There are four minima known for the M_7 cluster. The global minimum for this cluster is the pentagonal bipyramid, PBP(0), for the entire range of ρ_0 examined. It is also the only balanced structure that appears as a minimum of first-order saddle for this size cluster[10,23] [Fig. 8(a)]. The next higher-energy minimum is that of the capped octahedron, COCT(0), shown in Fig. 8(b). As the range of the potential is increased (ρ_0 decreased), this minimum changes into a second-order saddle. Next in energy is the incomplete stellated tetrahedron, IST(0), which can alternatively be described as a tricapped tetrahedron or as an IPB(0) capped on the 2–3–5 face [Fig. 8(c)]. This structure has the same point group as the COCT(0), and can be obtained from the latter by flattening it in the direction of the C_3 axis. Like the COCT(0), in fact, this structure also becomes a second-order saddle as ρ_0 is decreased. The critical point for this change is at $\rho_0 = 3.23$, somewhat higher than the similar change in the COCT(0), which is at $\rho_0 = 1.86$. See Table II. A symmetry-constrained saddle search showed that the *constrained* flattening process goes through a third-order saddle.

The highest-energy minimum is the skew structure, SKEW(0), which may be thought of as an IPB(0) capped on the 1–2–5 face or as a bicapped trigonal bipyramid [Fig. 8(d)]. It is the least symmetrical of the M_7 minima, having only a single twofold rotation axis. Because of its low symmetry this structure has the distinction of being the smallest homoatomic Morse or Lennard-Jones minimum to exhibit chirality. This geometry ceases to be a minimum for values

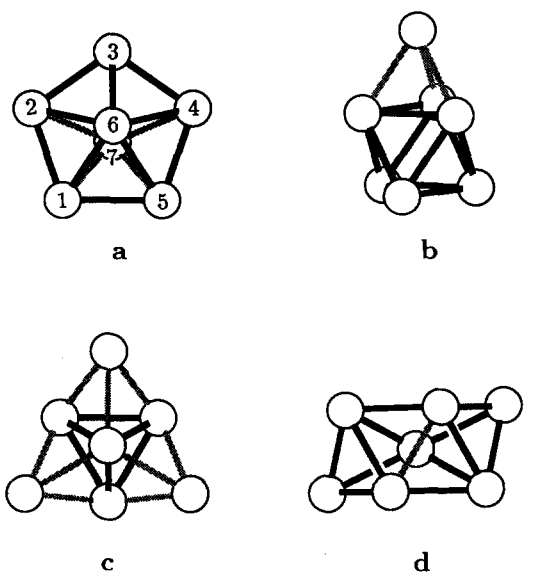

FIG. 8. The M_7 minima. (a) Pentagonal bipyramid, PBP(0). (b) Capped octahedron, COCT(0); the highlighted bonds emanate from the cap. (c) Incomplete stellated tetrahedron, IST(0); the highlighted bonds emanate from the three cap atoms. (d) Skew structure, SKEW(0); the diagonal highlighted bond is bisected by the sole symmetry element, a C_2 axis; the edges are highlighted for visualization purposes only.

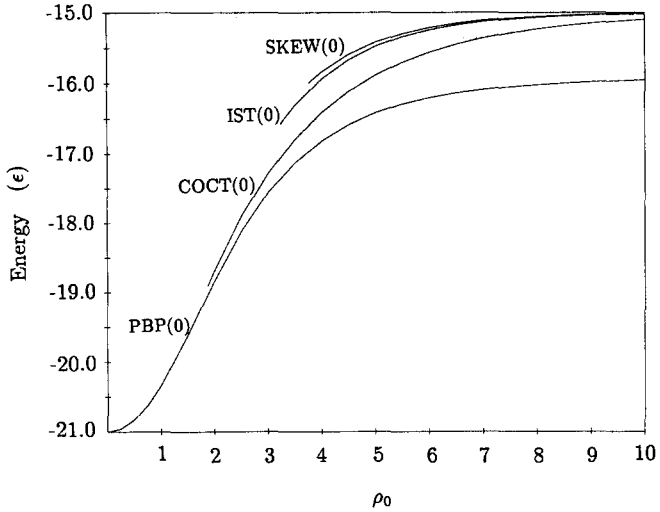

FIG. 9. Energies of the M_7 minima as a function of ρ_0.

of $\rho_0 < 3.74$, but rather than becoming a higher-order saddle, it appears to become an ordinary point on the potential surface. The process seems to be similar to the elimination of the IPB(0) minimum of the M_6 cluster.

Figure 9 and 10 for M_7 are analogous to Figs. 4 and 5 of the M_6 cluster. Hoare and Pal[20] found the same four minima for the Lennard-Jones potential,[20] but found three for the $\rho_0 = 3.0$ Morse potential. At this value of ρ_0 we would have expected them to find only the two lowest-energy structures, not the three that they reported. The most likely explanation for this discrepancy is that the IST(0) minimum that they found for the Lenneard-Jones cluster happened to be so close to the $\rho_0 = 3.0$ Morse structure IST(2) that the latter saddle was misclassified as a minimum.

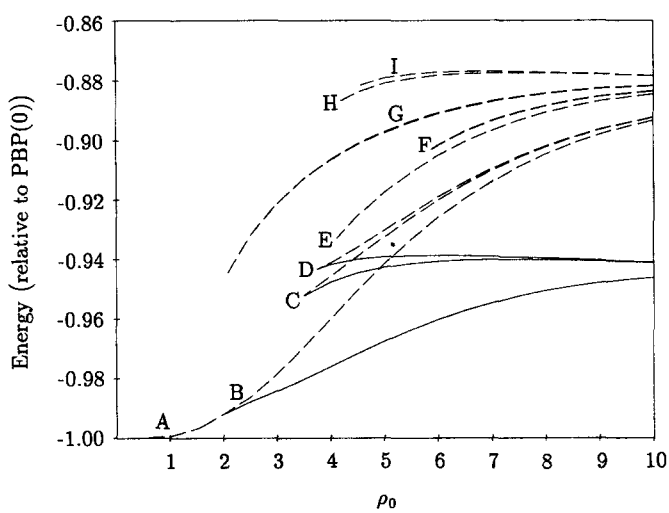

FIG. 10. Energies of the stationary points of M_7. The energies are relative to the pentagonal bipyramid, the global minimum. Solid curves: minima; dashed curves: first-order saddles. When a label refers to more than one structure, they will be listed in order of increasing energy. (A) S1.1 (b) and S1.1(a); (B) COCT(0) and S1.2dsd; (C) IST(0) and S2.3dsd; (D) SKEW(0) and S2.4dsd; (E) S2.2eb; (F) S1.4dsd and S1.3dsd; (G) S4.4dsd(a) and S4.4dsd(b); (H) S1.4eb; (I) S4.4eb.

TABLE IV. The M_7 saddles. The saddles below are named for the line on which they appear in Fig. 10 for large ρ_0.

Structure	Point group	Number	Range of ρ_0
S1.2dsd	C_s	5 040	$\rho_0 \geqslant 1.87$
	C_s	5 040	$1.67 \leqslant \rho_0 \leqslant 1.86$[a]
	C_{2v}	2 520	$\rho_0 \leqslant 1.66$[a]
S2.3dsd	C_s	5 040	$\rho_0 \geqslant 3.23$
S2.4dsd	C_1	10 080	$\rho_0 \geqslant 3.75$
S2.2eb	C_{2v}	2 520	$\rho_0 \geqslant 4.11$
S1.4dsd	C_1	10 080	$\rho_0 \geqslant 5.87$
S1.3dsd	C_s	5 040	$\rho_0 \geqslant 5.88$
S4.4dsd(a)	C_1	10 080	$\rho_0 \geqslant 3.73$
S4.4dsd(b)	C_{2v}	2 520	$\rho_0 \geqslant 3.73$
	C_{2v}	2 520	$2.72 \geqslant \rho_0 \geqslant 2.03$[b]
S1.4eb	C_1	10 080	$\rho_0 \geqslant 4.19$
S4.4eb	C_s	5 040	$\rho_0 \geqslant 4.56$

[a] This is a PBP(0)–PBP(0) isomerization via an edge rotation.
[b] This is a COCT(0)–COCT(0) isomerization via a complicated rearrangement.

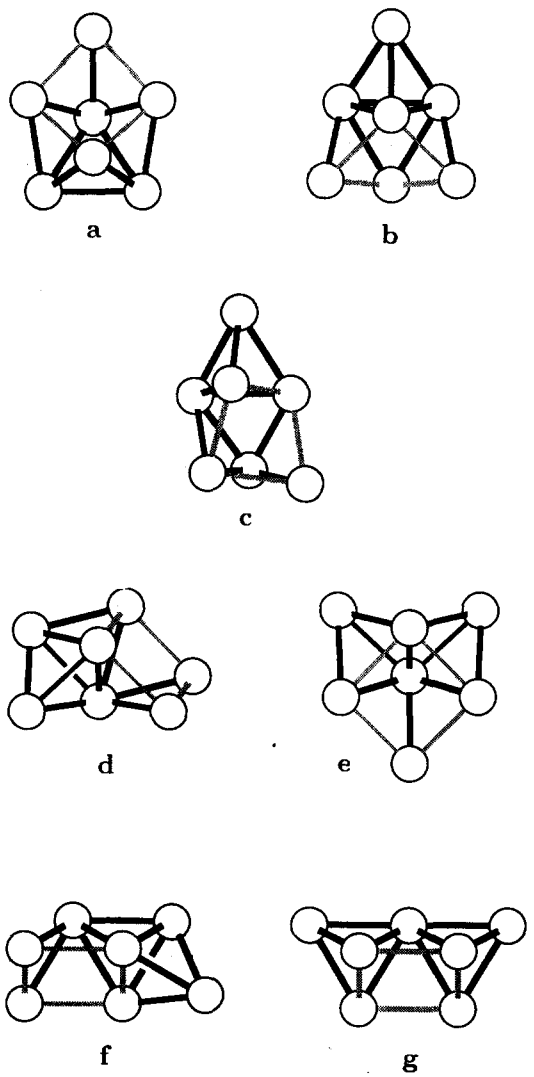

FIG. 11. Saddles for the DSD processes of M_7. All structures are shown for $\rho_0 = 10$. The highlighted bonds outline the critical face of each saddle. (a) S1.2dsd, (b)S2.3dsd; (c)S2.4dsd; (d) S1.4dsd; (e) S1.3dsd; (f) S4.4dsd (a); (g) S4.4dsd(b).

D. M_7 clusters: Rearrangement mechanisms

Most of the rearrangement mechanisms observed for the M_7 clusters utilize the DSD mechanism for $\rho_0 > 2$ although some of the higher-energy mechanisms are of the edge-bridging type. In this region of the potential we found ten first-order saddles. Eight of these can be identified with the saddles found by Davis, Beck, and Berry[26] and by Davis, Wales, and Berry[18] for a seven-particle Lennard-Jones cluster. The other two saddles had not been previously discovered, but they are indeed saddles for the Lennard-Jones potential as well. See Table IV.

The most important rearrangement for the M_7 cluster links the two lowest-energy minima, the PBP(0) and the COCT(0). The PBP(0) has ten equivalent edges which are the critical edges that break in a PBP(0)–COCT(0) DSD rearrangement. The transition state for this process retains the vertical mirror plane which contains the initial critical edge.

Other transition states of the seven-particle cluster have lower symmetry. In order to classify and describe them, we adopt the following naming procedure. The PBP(0)–COCT(0) transition state, shown in Fig. 11(a), will be denoted by "M7S1.2dsd." The "1.2" refers to the minima which the transition state connects: the lowest-energy and second-lowest-energy minima. The "S" stands for "saddle," and "M7" is for M_7. The "M7" is included to facilitate future comparison with other potentials and cluster sizes although it may be dropped if its omission introduces no ambiguity. A suffix is added to designate the reaction mechanism in most cases.

The COCT(0) obviously shares the M7S1.2dsd saddle with the PBP(0). The critical edge in this process can be any one of the three equivalent edges of the face of the octahedron upon which the cap atom resides. The other low-energy saddles are also connected to the COCT(0) minimum. These are M7S2.3dsd and M7S2.4dsd, shown in Figs. 11(b) and 11(c), respectively.

The next-highest-energy saddle is the M7S2.2eb structure, Fig. 12(b), which as one might expect is best described as an edge-bridged octahedron. At $\rho_0 = 4.11$ this saddle becomes second order.

The remaining high-energy saddles are pictured in Figs. 11 and 12, with the relevant information in Table IV. It is interesting to note that the four highest-energy DSD saddles can all be constructed by capping various faces of the M_6 saddle CSBP(1), which suggests that an *aufbau* building scheme as utilized by Hoare and Pal[20] in their search for Lennard-Jones minima may also be successfully used to construct many transition states.

All of these saddles and all but one of the minima disappear as ρ_0 decreases. Obviously, at least one minimum must always remain because the potential is attractive. If the remaining minimum has any distinct permutational isomers then there must also be at least one saddle. The structure of the M7S1.2 saddle remains intact even when the COCT(0) minimum disappears, but it begins to serve, via a similar pathway, as a direct connection between two pentagonal bipyramids. For smaller values of ρ_0 the sole remaining saddle becomes a capped trigonal prism, Fig. 12(a), consistent with

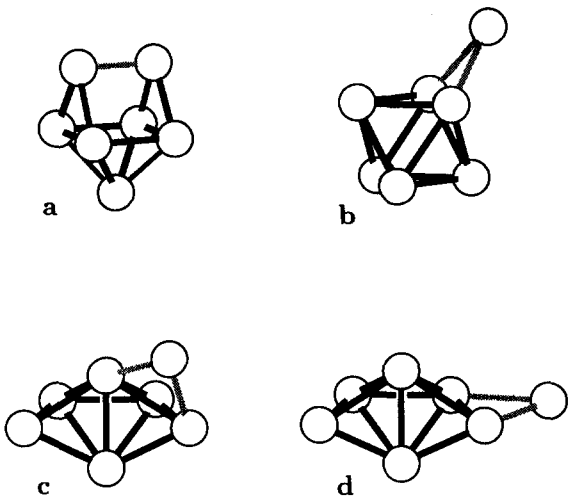

FIG. 12. Saddles for the edge rotation and edge-bridging processes of M_7. (a) S1.1er ($\rho_0 = 1.50$). The highlighted bond is the rotating edge. The remaining structures ($\rho_0 = 10.0$) are edge-bridging processes and the highlighted bonds emanate from the edge-bridge atom. (b) S2.2eb; (c) S1.4eb; (d) S4.4eb.

the remarks of the preceding paragraph. Throughout the $\rho_0 \leqslant 1.86$ region the 1–1 rearrangement is best described as an edge rotation. This mechanism may also be thought of as a concerted double DSD process.

VI. DISCUSSION

A. Lennard-Jones and high-ρ_0 Morse potentials

The reduced Morse potential, with its one free parameter, provides an isotropic model potential which is capable of displaying a much wider range of behavior than the commonly used Lennard-Jones interaction. When $\rho_0 = 6$ the reduced Morse potential closely mimics the Lennard-Jones one, although for other values of ρ_0 the two interactions are, in general, qualitatively very dissimilar.

All of the minima we located for high-ρ_0 surfaces are analogous to those found previously for Lennard-Jones clusters. The Lennard-Jones potential, with its r^{-6} decay, goes to zero more slowly than does the Morse potential with its exponential decay. Higher-energy structures, which tend to have fewer nearest neighbors and more second-nearest neighbors, are therefore slightly stabilized by the Lennard-Jones potential, but all the minima found present for one potential are present for the other. Furthermore, all saddles present in one potential are present in the other, again with a slight shift in energy. The only qualitative difference between the Morse potential at $\rho_0 = 6$ and Lennard-Jones is in the S1.3dsd and S1.4dsd saddles. The sequence of these saddles, which are very close together in energy, is interchanged in the Lennard-Jones approximation. This discrepancy is not of much importance since the saddles are very high and close in energy. See Fig. 13 for a comparison of the energies of the potentials. In light of these similarities, we expect the dynamics of a small Lennard-Jones cluster to differ only slightly from the dynamics of the corresponding Morse cluster with $\rho_0 = 6$. Qualitatively, they should be the same.

For both the six- and seven-atom clusters, the global

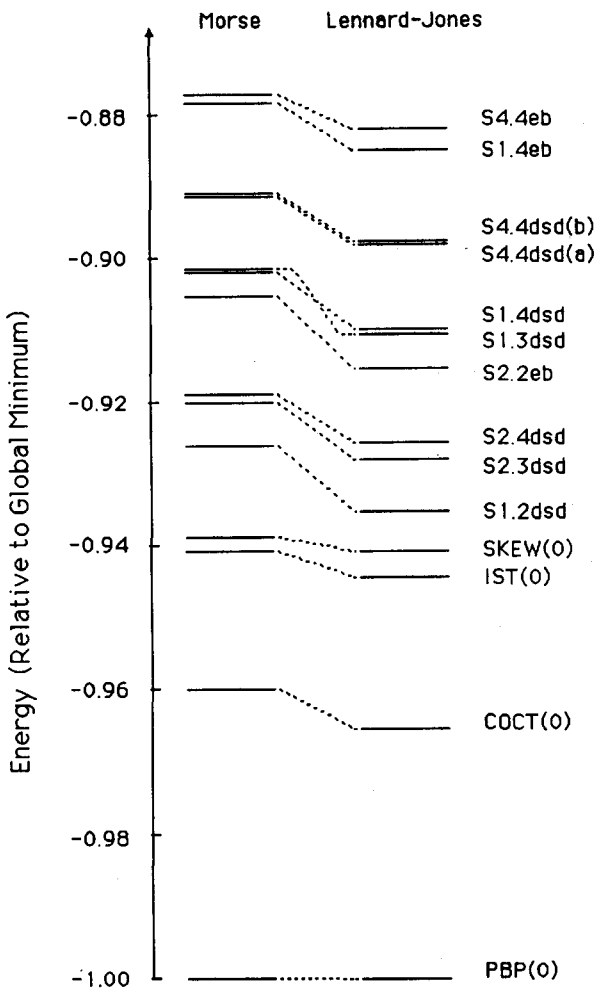

FIG. 13. Comparison of the dimensionless energies of the stationary points of the Morse potential ($\rho_0 = 6$) and the Lennard-Jones potential.

minimum remained the same deltahedral structure for all values of ρ_0. This is clearly explained in terms of nearest-neighbor distances. The M_6 octahedron has 12 nearest-neighbor pairs of atoms but only three second-nearest-neighbor pairs. The IPB(0), on the other hand, has five distinct sorts of neighbors. Optimization of the latter structure requires a delicate balance among the five different bonds, whereas optimization of the former is almost exclusively optimization of just one type of bond.

The nature of the M_7 minima is even easier to explain. Since the axial–axial distance of the PBP(0) is nearest neighbor, each of the three higher-energy minima has one fewer nearest-neighbor bond than the global minimum; hence they must be higher-energy structures. The ordering among these structures can be rationalized in a similar way.

B. Other clusters and potentials

There is no reason that the global minimum at a particular value of ρ_0 should be the global minimum at every value of ρ_0. In addition to the M_6 and M_7 clusters we did some optimization of the M_{13} cluster. This cluster is remarkable in that 13 particles can be arranged to form an icosahedron or

either one of the close-packed structures, the fcc cuboctahedron or the hcp anticuboctahedron.

The icosahedron has two sorts of nearest-neighbor contacts: those between the central atom and a surface atom, and those between adjacent surface atoms. There are 12 and 30 of these bonds, respectively. The radial bond is about 5% shorter than the surface bond. As ρ_0 increases, so does the competition between these two bonds. At $\rho_0 > 20$ the minimum turns into a third-order saddle, and as ρ_0 is increased further, it progresses through a 12th-, a 16th-, and ultimately a 21st-order saddle. At $\rho_0 = 10.0$ the energy of the icosahedron is -39.663ϵ. At $\rho_0 = 50.0$, 100.0, and 200.0 the energy of the structure is -16.812ϵ, -16.351ϵ, and -12.002ϵ, respectively. These show the correct asymptotic behavior, but the energies approach the limiting values much more slowly than in the smaller clusters.

The cuboctahedron (fcc) remains a first-order saddle throughout the physically relevant range of ρ_0. It connects two icosahedral minima in the physically interesting region of ρ_0. The mechanism for this rearrangement is a concerted sextuple DSD process of the surface atoms. It is very interesting to note that such a mechanism was first proposed to explain the rearrangements of $C_2B_{10}H_{12}$. *Ab initio* calculations showed[5] that the cuboctahedron is a higher-order saddle for $B_{12}H_{12}^{2-}$, and recent work has shown that the centered cuboctahedron is a true transition state both for argon and for the corresponding "trapped ion" cluster.[8] We did not pursue further our studies of the M_{13} cluster on this occasion.

C. Constructing the molecular symmetry group

We now show how the effective molecular symmetry group of a cluster can be determined from a knowledge of the connectivities of the minima of the potential surface. For a review of the molecular symmetry group, see Bunker[27] and references therein.

If a nonlinear system is confined to a particular potential well on the time scale of the observation, then it can be shown that its effective molecular symmetry group is isomorphic to the molecular point group of that well. If the system can exhibit large-amplitude vibrational motions, or if it can escape the potential well and visit other minima, then the point group must be replaced by the effective molecular symmetry group to provide an adequate description of the system. The molecular symmetry groups are subgroups of the complete nuclear permutation-inversion groups. This latter group is just the direct product of the nuclear permutation group[28] ($\mathcal{S}_N$ for an N-atom cluster), and the inversion group, $(\mathcal{E}, \mathcal{E}^*)$, where $\mathcal{E}^*$ represents the operator that inverts all position and momentum vectors through the center of mass and $\mathcal{E}$ is the identity.

At very low total energies the M_6 cluster has motions confined to small-amplitude vibrations within an octahedral minimum. Its corresponding molecular symmetry group is therefore isomorphic to the point group of the well, O_h. The question then arises: "How much energy must the cluster have in order to escape that particular octahedral well and visit any other?" That is, at what energy does the effective molecular symmetry group become the complete nuclear permutation-inversion group $\mathcal{S}_6 \otimes (\mathcal{E}, \mathcal{E}^*)$? We must answer this question in two parts: one for $\rho_0 > 4.10$ and one for $\rho_0 \leqslant 4.10$.

When $\rho_0 > 4.10$, the lowest saddle leads to any of 12 equivalent IPB(0) intermediates. Unless the cluster has sufficient energy to traverse the next higher saddle, the only way out of this well is back into the OCT(0) well. Once the energy has increased enough, the IPB(0) may undergo any of four degenerate DSD processes via the CSBP(1) saddles. We shall now demonstrate that once this transition is allowed to occur, every OCT(0) minimum becomes accessible to the cluster. We do this by showing that we can interchange the atoms on any edge of the octahedron.

Let the skeleton of the octahedron have vertices numbered as in Fig. 3(a). Furthermore, let us begin with atom one at site one, atom two at site two, etc. A DSD process on the 1–4 edge will result in an IPB(0) skeleton labeled as in Fig. 3(b). If we now preform a DSD process on the 2–5 edge and bring the pseudorotated[29] skeleton back to its reference orientation we see that the atom will have changed location on the fixed IPB(0) skeleton; thus atom one moves to site two and vice versa, atom five moves to site three, atom three moves to site six, and atom six moves to site five. The entire process can be written as the permutation[28] $\mathbf{p}_{6a} = (12)(365)$. It is evident that $\mathbf{p}_{6a}^3 = (12)$, so if we perform another DSD process on the 5–6 edge to recover the octahedron we see that we have effected an edge rotation. Since we can place the octahedron in any orientation we desire, we can sequentially interchange the atoms on any edge and thereby produce any nuclear permutation of the original OCT(0). Thus, once the cluster has enough energy to overcome the CSBP(1) saddle the effective molecular symmetry group becomes the complete nuclear permutation-inversion group for $\rho_0 > 4.10$ provided that the time scale of observation is long enough.[29]

For $\rho_0 \leqslant 4.10$ the proof is slightly more complicated because we must now explicitly take rotations into account. It is easily shown that the generators $\mathbf{r}_{4z} = (1234)$ and $\mathbf{r}_3 = (126)(345)$ generate a group isomorphic to O, the group of rotations of the octahedron, so that we may use these generators to place the octahedron into any orientation that we may require. These generators correspond to, but are not identical with, the point group operations C_{4z} and one of the C_3. These are the same generators we would need in the case of $\rho_0 > 4.10$ to bring the desired edge into the proper location.

The transition mechanism for the longer-range potential is the face rotation, for which the one generator $\mathbf{p}_{6b} = (345)$ will suffice. Now $\mathbf{r}_{4z}\mathbf{p}_{6b} = (123)(45)$ so that, as before, $(\mathbf{r}_{4z}\mathbf{p}_{6b})^3 = (45)$ and this case is proved.

We could have written a shorter path in both of these cases if we had utilized the other available transitions, which can be written as products of the rotations and the sole rearrangement permutation, but to make the algorithm as generally applicable as possible, we wished to conduct the proof using as few permutation generators as necessary. In the preceding cases, and in the cases of M_7 which follow, we show by construction that the generators of the rotational subgroup of the point group and just one nonrotational permu-

tation element are sufficient to generate the complete nuclear permutation-inversion group. This will not, in general, be true for more complex systems.

For M_7 we have two edges that we must be able to rotate in order to obtain the molecular symmetry group $\mathscr{S}_7 \otimes (\mathscr{E}, \mathscr{E}^*)$. One of these bonds is any of the five edges between adjacent equatorial atoms and the other is any of the ten between a polar atom and an equatorial atom. Let the PBP(0) skeleton be labeled as in Fig. 8(a) and let each atom be labeled with the same number as the site it initially occupies. Two generators are sufficient to produce any rotation. They are $\mathbf{r}_{5z} = (12345)$ which corresponds to a C_{5z} rotation and $\mathbf{r}_{2x} = (25)(34)(67)$ which corresponds to a C_{2x} rotation. These generators produce a group isomorphic to D_5, the group of rotations of the pentagonal bipyramid.

When $\rho_0 > 1.86$, the lowest-energy saddle connects the PBP(0) with the COCT(0). The structure can return to the PBP(0) either by reversing its original path, thereby recovering the original PBP(0), or else it may take one of two alternate paths that leads to distinct but equivalent PBP(0) wells. These two paths result in the permutations $\mathbf{p}_{7a} = (2746)$ and $\mathbf{p}_{7b} = (3657)$. Now $\mathbf{r}_{5z}^2\mathbf{p}_{7a} = (13527)(46)$ so that $(\mathbf{r}_{5z}^2\mathbf{p}_{7a})^5 = (46)$, a polar-equatorial edge rotation. Also, $\mathbf{r}_{2x}\mathbf{p}_{7a}\mathbf{r}_{5z}^2\mathbf{p}_{7a} = (14567)(23)$ which leads to $(\mathbf{r}_{2x}\mathbf{p}_{7a}\mathbf{r}_{5z}^2\mathbf{p}_{7a})^5 = (23)$, an equatorial edge rotation, thus completing the proof for the $\rho_0 > 1.86$ case and confirming the previous analysis of Davis, Wales, and Berry[18] for a Lennard-Jones Ar_7 cluster.

When $\rho_0 \leqslant 1.86$, the only minimum that remains is the global minimum pentagonal bipyramid and the one PBP(0)–PBP(0) saddle. As described in Sec. V, this rearrangement is an edge rotation and the permutation may be written $\mathbf{p}_{7c} = (3756)$. It is easily shown that $\mathbf{p}_{7c}\mathbf{r}_{5z}\mathbf{r}_{2x}\mathbf{p}_{7c} = (12)$ and that $(\mathbf{r}_{5z}^2\mathbf{p}_{7c})^5 = (56)$. Therefore, once the M_7 system is able to surpass the first saddle, then every PBP(0) permutation is feasible.

VII. CONCLUSIONS

In the present work we have developed a procedure for the systematic investigation of the most important features of multidimensional potential-energy surfaces. The procedure has been demonstrated through the use of six- and seven-atom clusters with a pairwise additive Morse potential. The reduction law derived for this potential leaves us with just one variable parameter that governs the range of the interactions, so that there is a single degree of flexibility, in contrast to the reduced Lennard-Jones potential, which has none. Hence we have studied the changes in the topologies of the potential-energy surfaces with the change in range of the interatomic potential. This approach provides a convenient means for visualizing and classifying rearrangement in a wide range of clusters, from inert gases to transition metals. It is powerful, not only because many systems may be well represented by the isotropic, pairwise-additive potential (for example, inert-gas, gold, and silver clusters), but also because the method can be extended to be used with anisotropic, many-body interactions in other systems.

Although we used the reduced Morse potential as the means of studying the relationship between the range of pair interactions and the features of multidimensional potential-energy surfaces, we can expect that the qualitative results will hold true in the general case of arbitrary attractive pair interactions. In general, as the range of interaction decreases, the number of local minima increases, mainly due to the decreasing importance of the second-nearest-neighbor interactions. As the range of the interactions increases, the higher-energy minima are successively "swallowed up" by the lower-energy minima until only the lowest-energy minimum is left. Stillinger and Weber[30] first hypothesized this behavior and utilized it in their derivation of the "ant–lion" method of finding global minima. The range of the pair interaction also has a pronounced effect on the reaction mechanisms and saddle structures. Our findings with the variation of range of the Morse potential can be expected to be fairly general on at least two grounds: Results obtained[31] with the Gupta potential[32] (more general than a pair potential) are very similar to those from the Morse and Lennard-Jones potential with essentially the same range; and the generalization of the Lennard-Jones 6–12 potential into $V_{LJ} = A(1 - (r/r_0)^{-n})^2$ also shows results parallel with ours.[33]

One may ask how close to physical realization might the idea of variable-range potentials be brought. There is an example that comes to mind, namely the Debye potential in ionic solutions, whose range depends on the ionic strength. We might expect, for example, different crystal structures for precipitates formed from solutions of the same concentration of precipitating material but different ionic strength, as a result of the different effective potentials between the ions.

For the systems considered in detail here, regardless of the strength or range of the potential, if an M_6 or M_7 cluster has sufficient energy to access different permutational isomers of the same global minimum, it can also access *all* of its permutational isomers. The effective molecular symmetry then becomes the complete nuclear permutation-inversion group. A discussion of the topology of these potential-energy surfaces is currently being prepared and will be presented in a future paper.

This study suggests the following fascinating and fundamental question: How do the static features of the multidimensional potential-energy surface determine the sort of dynamics exhibited by the system? We are at present performing molecular-dynamics simulations on the aforementioned Morse systems at various values of ρ_0 in order to gain a better understanding of the nature of this relationship.

ACKNOWLEDGMENTS

P.A.B. wishes to thank Dr. Heidi Davis for many helpful discussions. P.A.B. would also like to thank John Rose and R. J. Hinde. D. J. W. thanks the Lindemann Trust for the Fellowship which he held during 1989 at The University of Chicago. This work was supported in part by a grant from the National Science Foundation.

APPENDIX

Here we present the second derivatives of the Morse potential in their reduced form. For the sake of convenience,

we also include here the Morse potential itself as well as the gradient. The reduced units follow the same subscript convention as presented in Sec. III and are defined as follows:

$$\rho_{ij} = r_{ij}\beta \quad \text{and} \quad \rho_0 = r_0\beta,$$
$$\hat{x}_{ij} = x_{ij}\beta, \quad \text{etc.},$$
$$\hat{V}(\rho_0;\rho) = V(r_0,\beta;r)/\epsilon.$$

With these definitions, the reduced potential and its derivatives become

$$\hat{V} = \sum_{i<j} g_{ij}(g_{ij} - 2), \tag{A1}$$

$$\frac{\partial \hat{V}}{\partial \hat{x}_n} = -2\sum_{i\neq n} \frac{\hat{x}_{ni}}{\rho_{ni}} g_{ni}(g_{ni} - 1), \tag{A2}$$

$$\frac{\partial^2 \hat{V}}{\partial \hat{x}_n^2} = 2\sum_{i\neq n} \frac{g_{ni}}{\rho_{ni}} \left\{ \left[\left(\frac{\hat{x}_{ni}}{\rho_{ni}} \right)^2 - 1 \right] (g_{ni} - 1) + \frac{\hat{x}_{ni}^2}{\rho_{ni}} (2g_{ni} - 1) \right\}, \tag{A3}$$

$$\frac{\partial^2 \hat{V}}{\partial \hat{x}_n \partial \hat{y}_n} = 2\sum_{i\neq n} \frac{\hat{x}_{ni}\hat{y}_{ni}}{\rho_{ni}^2} g_{ni} \times \left[\frac{1}{\rho_{ni}} (g_{ni} - 1) + (2g_{ni} - 1) \right], \tag{A4}$$

$$\frac{\partial^2 \hat{V}}{\partial \hat{x}_n \partial \hat{y}_m} = 2\frac{\hat{x}_{nm}\hat{y}_{nm}}{\rho_{nm}^2} g_{nm} \left[\frac{1}{\rho_{nm}} (g_{nm} - 1) + (2g_{nm} - 1) \right], \tag{A5}$$

$$\frac{\partial^2 \hat{V}}{\partial \hat{x}_n \partial \hat{x}_m} = 2\frac{g_{nm}}{\rho_{nm}} \left\{ \left[\left(\frac{\hat{x}_{nm}}{\rho_{nm}} \right)^2 + 1 \right] (g_{nm} - 1) - \frac{\hat{x}_{nm}^2}{\rho_{nm}} (2g_{nm} - 1) \right\}, \tag{A6}$$

where we have defined

$$g_{ij} = e^{\rho_0 - \rho_{ij}}. \tag{A7}$$

Since the potential is single valued the surface consists of only one sheet. It therefore has continuous first derivatives everywhere of interest and the Hessian is a symmetric matrix. The obvious substitutions of Cartesian coordinates will yield the other two equations for the gradient and the other eight equations for the second derivatives.

To express these equations in the nonreduced form, one should perform the following procedure. First, redefine g_{ij} to $g_{ij} = e^{-\beta(r_{ij} - r_0)}$ in Eqs. (A1)–(A6) and remove the hats from all the variables. Replace every occurrence of the variable ρ with r while preserving the subscripts. Next, multiply Eq. (A1) by ϵ and multiply Eqs. (A2)–(A6) by $\beta\epsilon$. Lastly, in Eqs. (A3)–(A6) multiply the $(2g - 1)$ term by β.

[1] J. R. Reimers and R. O. Watts, Chem. Phys. **85**, 83 (1984); R. N. Barnett, U. Landman, C. L. Cleveland, and J. Jortner, J. Chem. Phys. **88**, 4421 (1988).
[2] P. M. Morse, Phys. Rev. **34**, 57 (1929).
[3] J. E. Lennard-Jones, Proc. R. Soc. London, Ser. A **106**, 463 (1924).
[4] W. N. Lipscomb, Science **153**, 373 (1966).
[5] D. J. Wales and A. J. Stone, Inorg. Chem. **26**, 3845 (1987); D. J. Wales, D. M. P. Mingos, and Z. Lin, *ibid.* **28**, 2754 (1989); D. J. Wales and D. M. P. Mingos, Polyhedron **15**, 1933 (1989).
[6] R. B. King, Inorg. Chim. Acta **49**, 237 (1981).
[7] B. F. G. Johnson, J. Chem. Soc. Chem. Commun. **1986**, 27.
[8] D. J. Wales, J. Chem. Phys. **91**, 7002 (1989).
[9] D. J. Wales, Chem. Phys. Lett. **166**, 419 (1990).
[10] D. J. Wales, J. Am. Chem. Soc. **112**, 7908 (1990).
[11] K. P. Huber and G. Herzberg, *Constants of Diatomic Molecules* (Van Nostrand Reinhold, New York, 1979).
[12] G. Herzberg, *Spectra of Diatomic Molecules* (Van Nostrand Reinhold, New York, 1950).
[13] G. Apai, J. F. Hamilton, J. Stohr, and A. Thompson, Phys. Rev. Lett. **43**, 165 (1979); H. Purdum, P. A. Montano, G. K. Shenoy, and T. Morrison, Phys. Rev. B **25**, 4412 (1982); P. A. Montano, W. Schulze, B. Tesche, G. K. Shenoy, and T. I. Morrison, *ibid.* **30**, 672 (1984).
[14] D. Tománek, S. Mukherjee, and K. H. Benneman, Phys. Rev. B **28**, 665 (1983).
[15] D. ter Haar, Phys. Rev. **70**, 222 (1946).
[16] A. Rodger and P. E. Schipper, Chem. Phys **107**, 329 (1986).
[17] C. J. Cerjan and W. H. Miller, J. Chem. Phys. **75**, 2800 (1981).
[18] H. L. Davis, D. J. Wales, and R. S. Berry, J. Chem. Phys. **92**, 4308 (1990).
[19] ACES (Advanced Concepts in Electronic Structure)—An *ab initio* program system, authored by R. J. Bartlett, G. D. Purvis, G. B. Fitzgerald, R. J. Harrison, Y. S. Lee, W. D. Laidig, S. J. Cole, G. W. Trucks, D. H. Magers, E. A. Salter, C. Sosa, M. Rittby, S. Pal, and J. F. Stanton.
[20] M. R. Hoare and P. Pal, Adv. Phys. **20**, 161 (1971); M. R. Hoare, in *Advances in Chemical Physics, Vol. V*, edited by I. Prigonine and S. A. Rice (Wiley, New York, 1979).
[21] T. Komoda. Jpn. J. Appl. Phys. **7**, 27 (1968); J. Farges, B. Raoult, and G. Torchet, J. Chem. Phys. **59**, 3454 (1973); J. Farges, M. F. de Feraudy, B. Raoult, and G. Torchet, *ibid.* **78**, 5067 (1983); **84**, 3491 (1986); **84**, 3491 (1986); L.B. Knight, Jr. and R. W. Woodward, *ibid.* **79**, 5820 (1983).
[22] K. P. Hall, D. I. Gilmour and D. M. P. Mingos, J. Organomet. Chem. **268**, 275 (1984); Y. Ohta, J. Phys. Soc. Jpn. **57**, 2609 (1988).
[23] J. Leech, Math. Gazette **1957**, 41 (1981).
[24] R. E. Stanton and J. W. McIver, Jr., J. Am. Chem. Soc. **97**, 3632 (1975).
[25] D. M. P. Mingos and D. J. Wales, *Introduction to Cluster Chemistry* (Prentice-Hall, New York, 1990).
[26] R. S. Berry, H. L. Davis, and T. L. Beck, Chem. Phys. Lett. **147**, 13 (1988).
[27] P. R. Bunker, in *Vibrational Spectra and Structure, Vol.* 3, edited by J. R. Durig (Marcel Dekker, New York, 1975).
[28] A good elementary treatment of group theory and permutation groups can be found in J. B. Fraleigh, *A first Course in Abstract Algebra* (Addison-Wesley, Reading, MA, 1982). For a more in-depth treatment, see, for example, M. Hamermesh, *Group Theory* (Addison-Wesley, Reading, MA, 1962), or J.-Q. Chen, *Group Representation Theory for Physicists* (World Scientific, Teaneck, 1989).
[29] R. S. Berry, Rev. Mod. Phys. **32**, 447 (1960).
[30] F. H. Stillinger and T. A. Weber, J. Stat. Phys. **52**, 1429 (1988).
[31] S. Sawada and S. Sugano, Z. Phys. D **12**, 189 (1989); S. Sawada, in *Microclusters*, edited by S. Sugano, Y. Nishina, and S. Ohnishi (Springer, New York, 1987).
[32] R. P. Gupta, Phys. Rev. B **23**, 6265 (1981).
[33] F. H. Stillinger and D. K. Stillinger, J. Chem. Phys. **93**, 6106 (1990).